Density relaxation of a near-critical fluid in response to local heating and low frequency vibration in microgravity

Arnaud Jounet
IMFT, UFR MIG, Université Paul Sabatier, 118 Route de Narbonne, 31062 Toulouse Cedex, France
and CNES, 18 Avenue Edouard Belin, 31405 Toulouse Cedex 04, France
(Received 29 June 2001; published 19 February 2002)

The response of a confined near-critical fluid to local heating in the presence of vibration is studied by means of two-dimensional numerical simulations of the compressible and unsteady Navier-Stokes equations written for a van der Waals fluid. As in the experiments performed two years ago onboard the Mir orbital station, two different regimes of density distribution are observed. For sufficiently low frequency and high amplitude vibration, two thermal plumes develop from the heat source along the vibration axis. Otherwise (higher frequency and/or lower amplitude), density inhomogeneities caused by heating stay around the heat source. For this regime, the pair of vortices created in each half period absorbs the preceding one, while it is convected away for the double-plume regime. As time goes on, this process repeats, with a lateral extension of the low density region. At lower frequencies, instabilities appear in the flow, thus corroborating again microgravity experiments.

DOI: 10.1103/PhysRevE.65.037301 PACS number(s): 05.70.Jk, 47.15.Rq, 47.20.Bp, 47.32.Cc

In 1990, three different teams [1–4] pointed out the role of the large compressibility of near-critical fluids in the rapid thermal relaxation observed in microgravity [5]. This was a major finding because experimental measurements were opposed to the critical slowing down theory, which predicted that thermal equilibration in near-critical fluids should be achieved more slowly when approaching the liquid-vapor critical point due to the critical decrease of the thermal diffusivity D_T'. The mechanism involved was called the piston effect or the adiabatic effect and works as follows. When submitted to local temperature increase, a near-critical fluid expands strongly by dilation. As in the piston process, the rest of the fluid in the container is then compressed and adiabatically heated due to the thermal conversion of this pressure rise. Since the fluid is highly compressible, rapid thermal relaxation occurs on a time scale much shorter than that of thermal diffusion. In the 1990s, further insights [6–8] were brought to the piston effect and critical speeding up theories, and more experimental evidence of the piston effect was obtained [9–14]. Furthermore, it was shown that the piston effect was still efficient on the ground despite some specific coupling with natural convection [15,16]. Some unusual flow patterns were also reported due to the presence of steep density gradients generated near the heat sources and to the low thermal and kinematic diffusion coefficients of fluids near their critical point. In addition, a specific effort was made to characterize the density relaxation process, since it remains driven by the long-lasting diffusion phenomenon [12,14,17]. In relation to these problems, Beysens [18] and Zappoli *et al.* [19] have recently reported the results of measurements performed on the Mir station two years ago. Observations were related to the development of density inhomogeneities after a few periods of controlled vibration and on longer times in a noninsulated cylindrical cell heated by an immersed thermistor. But since flow fields could not be measured, the observed behaviors still needed some clarification. For this purpose, we present in this paper the results of numerical simulations based on the Navier-Stokes equations.

We consider a two-dimensional square cavity filled with near-critical CO_2. The heating source, located at the center of the domain, provides constant power while all the boundaries are maintained at the initial temperature [6,8,13,19]. Vibration is parallel to one axis of the box ($\vec{e}_y$). Initially, the fluid is motionless at the critical density and at thermal equilibrium close above its critical temperature. The van der Waals equation of state is used to take into account the anomalous behavior of equilibrium parameters close to the critical point, especially the divergence of the isothermal compressibility κ_T', that of the dilation coefficient α_P', and that of the specific heat at constant pressure C_P'. With the additional use of a diverging law accounting for the thermal conductivity divergence [Eq. (6) below], this model was shown to be qualitatively correct and to reflect the strong thermomechanical couplings specific to near-critical fluids [13]. On the vibration time scale, the dimensionless conservation equations for mass, momentum, and energy considered in our model [7,21], plus the van der Waals equation, are

$$\vec{\nabla}\cdot\vec{v}=\frac{(1-b\rho)dP^{(0)}/dt-(\gamma_0/\mathrm{Pr}_0\mathrm{Re}_0)\vec{\nabla}\cdot[\lambda\vec{\nabla}T]}{-\gamma_0(P^{(0)}+a\rho^2)+2a\rho^2(1-b\rho)}, \quad (1)$$

$$\frac{\partial(\rho\vec{v})}{\partial t}+\vec{\nabla}\cdot(\rho\vec{v}\otimes\vec{v})=-\vec{\nabla}\Pi+\frac{1}{\mathrm{Re}_0}[\nabla^2\vec{v}+\tfrac{1}{3}\vec{\nabla}(\vec{\nabla}\cdot\vec{v})]+\rho A\sin(2\pi t)\vec{e}_y, \quad (2)$$

$$\frac{\partial(\rho T)}{\partial t}+\vec{\nabla}\cdot(\rho\vec{v}T)=\frac{1}{\mathrm{Pr}_0\mathrm{Re}_0}\vec{\nabla}\cdot[\lambda\vec{\nabla}T]+r+\frac{(\gamma_0-1)}{\gamma_0}\times(1-b\rho)\left(\frac{dP^{(0)}}{dt}-2a\rho^2\vec{\nabla}\cdot\vec{v}\right), \quad (3)$$

$$P^{(0)}=\frac{\rho T}{1-b\rho}-a\rho^2. \quad (4)$$

In this system, the acoustic filtering procedure [22] has been applied for numerical reasons, leading to pressure splitting. Π represents the dynamic pressure and $P^{(0)}$ the homogeneous part of the pressure; hence

$$\vec{\nabla} P^{(0)} = \vec{0}. \tag{5}$$

Nondimensionalization was achieved as follows:

$$\vec{x}' = L' \vec{x}, \quad t' = \frac{L'}{U'} t, \quad \vec{v}' = U' \vec{v},$$

$$P^{(1)'} = \rho_c' U'^2 P^{(1)} \quad (\vec{\nabla}\Pi = \gamma_0 \mathrm{Ma}^2 \vec{\nabla} P^{(1)}),$$

$$P^{(0)'} = \rho_c' R' T_c' P^{(0)}, \quad T' = T_c' T, \quad \rho' = \rho_c' \rho,$$

$$r' = r_0' r \quad \text{with} \quad r_0' = \rho_c' R' T_c' U' / (\gamma_0 - 1) L',$$

$$\lambda' = \lambda_0' \lambda = \lambda_0' [1 + \Lambda (T-1)^{-1/2}], \tag{6}$$

where the reference velocity U' is chosen such that

$$U' = f' L'. \tag{7}$$

In the above relations, the prime denotes dimensional parameters (ρ_c' and T_c' are the critical density and temperature, R' the perfect gas constant, L' the characteristic length of the cavity, and f' the vibration frequency), $\Lambda = 0.75$ is a constant, and $\mathrm{Ma} = U'/c_0'$, with $c_0' = \sqrt{\gamma_0 R' T_c'}$ a specific sound velocity. The dimensionless parameters present in Eqs. (1)–(3) are defined as

$$\gamma_0 = \frac{C_{p_0}'}{C_{v_0}'}, \quad \mathrm{Pr}_0 = \frac{\mu_0' C_{p_0}'}{\lambda_0'},$$

$$\mathrm{Re}_0 = \frac{\rho_c' U' L'}{\mu_0'}, \quad A = \frac{A' L'}{U'^2}$$

(γ_0 is the ratio of specific heats in a reference state far away from the critical point, Pr_0 a specific Prandtl number with μ_0' the characteristic dynamic viscosity, Re_0 a specific Reynolds number, and A the dimensionless vibration acceleration). $a = 9/8$ and $b = 1/3$ are the van der Waals universal coefficients. In Eq. (3), note that r accounts for the heat source at the center of the cavity. In the presence of the homogeneous oscillating acceleration field [Eq. (2)], this term allows the onset of buoyant (vibrational) convection by causing the density differences in the fluid. It is constant during the computations. Typically, its value for a two-dimensional 10-mm-wide cavity corresponds to $\dot{Q}_l' = 0.11$ W m^{-1} (this is equivalent to a power $P' = 0.82$ mW in the experimental cell of the Alice facilities [19]). Vibrations are imposed after a delay Δt_{vib} such that $\Delta t_{vib}' = 1.25$ sec.

Numerically, the system (1)–(5) with its initial and boundary conditions is solved by means of the SIMPLER algorithm applied after finite volume discretization [23]. During the iterative procedure, the static pressure $P^{(0)}$ is calculated through the total mass conservation and the equation of state by the relation

$$\frac{\partial P^{(0)}}{\partial t} = \frac{\int_V \rho \alpha_P (\partial T/\partial t) dV}{\int_V \rho \kappa_T dV}. \tag{8}$$

Despite strong thermomechanical coupling, this then allows the stable calculation of the density by inversion of the van der Waals equation.

The primary aim of this study was to retrieve the two different regimes of density distribution observed experimentally [18,19]. This was done by varying the frequency and amplitude of vibration at 1 K above T_c' ($\Delta T_i' = 1$ K). The two frequencies used in our calculations (0.8 Hz and 1.8 Hz) were chosen in agreement with experimental data [24]. For $f' = 0.8$ Hz and $A' = 10$ m s^{-2}, Fig. 1(a) shows that two (quasi)symmetrical thermal plumes develop in the direction of vibration. Note in this figure the presence of a boundary layer along the walls, before convective or diffusive transport from the heat source has reached those regions: this is the stamp of the piston effect, since it reflects a homogeneous rise of the bulk density (then, boundary layers form by diffusion due to the thermal boundary conditions). The regime of perpendicular extension of the heated-lighter fluid was obtained for higher frequency and lower amplitude of vibration [Fig. 1(b)]. It should be mentioned that in both cases negative density changes develop from the heat source ($\Delta\rho' \sim -30$ kg m^{-3}) while cooling from the sidewalls provokes positive density changes in the boundary layers ($\Delta\rho' \sim +1$ kg m^{-3}). To understand the mechanisms responsible for the opposite behaviors pointed out in Fig. 1, we have to resort to the flows developing in these two situations.

First consider the double-plume regime at the initial times of vibration. Figure 2 shows the velocity field during the first period (the arrow length is scaled to the local velocity amplitude, the order of magnitude of which is $v' \sim 1$ mm s^{-1}). During this period, two symmetrical convective rolls first form by viscous coupling due to the buoyant-vibrational force associated with the density gradients that have developed from the heat source. Those vortices are first convected downward (upper fields of Fig. 2) and their cores correspond to the head of the lower plume. After half a period, the vibration direction is reversed and two new vortices are generated upward, corresponding to the upper plume, while the lower vortices are still active (lower fields). Later, the vortices generated during this period are convected further or absorbed by the new ones (not shown). Older density inhomogeneities are then progressively spread along the horizontal boundaries (with lower gradients because of convective mixing), while the core of the double plume remains continuously fed (not shown). When the plot of isodensity lines is adequately selected, this leads to the field of Fig. 1(a) at $t = \Delta t_{vib} + 5$, which roughly corresponds to that obtained in Refs. [18,19] by interferometry.

The flow field obtained for lower amplitude and higher frequency vibration is shown in Fig. 3 (magnification around the heat source). During the first half period, a pair of vortices also develop from the heat source, but since the buoyant-vibrational force has decreased and since less time has

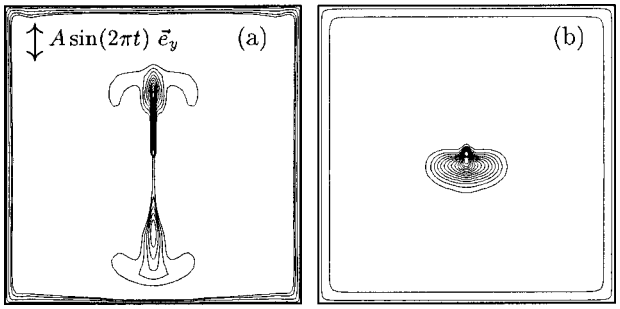

FIG. 1. Instantaneous density fields when (a) $f'=0.8$ Hz and $A'=10\ \mathrm{m\,s^{-2}}$, (b) $f'=1.8$ Hz and $A'=1\ \mathrm{m\,s^{-2}}$, after five (a) and ten (b) periods of oscillation ($t'=\Delta t'_{vib}+6.25$ sec and $t'=\Delta t'_{vib}+5.55$ sec, respectively). In both cases, $L'=10$ mm and $\Delta T'_i=1$ K. In the following, case (a) will be referred to as the low frequency or double-plume regime and case (b) as the higher frequency regime.

elapsed, these rolls do not have time to flow away. Then, when the vibration force changes direction, the new vortices that are generated with opposite inner rotations absorb the old ones, as illustrated in Fig. 3. This phenomenon recurs every half period of vibration and the double-plume structure cannot develop. For longer times, density inhomogeneities thus stay located around the heat source (Fig. 4). As in the experiment performed on the Mir station [18], our calculations evidence a lateral extension of those inhomogeneities. This latest pattern can be explained by the interplay between the dying and emerging vortices during the flow inversion phase, since a small lateral deviation of the cores of the new vortices occurs every half period. As density inhomogeneities are transported by the vortex flows, they also move laterally.

Concerning the double-plume regime, we have explored the short time period but some other behaviors have also been observed on medium and long time scales [18,19].

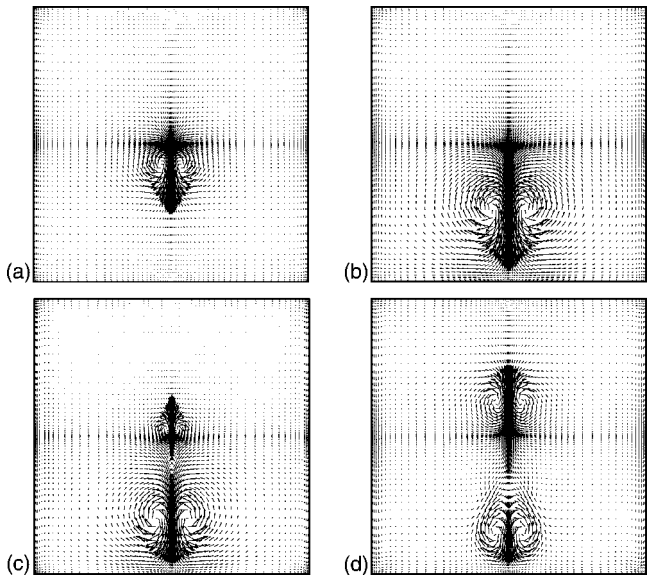

FIG. 2. Double-plume regime during the first period of vibration. Velocity fields in the case of Fig. 1(a) at times (a) $t=\Delta t_{vib}+0.2$, (b) $t=\Delta t_{vib}+0.5$, (c) $t=\Delta t_{vib}+0.7$, and (d) $t=\Delta t_{vib}+1$.

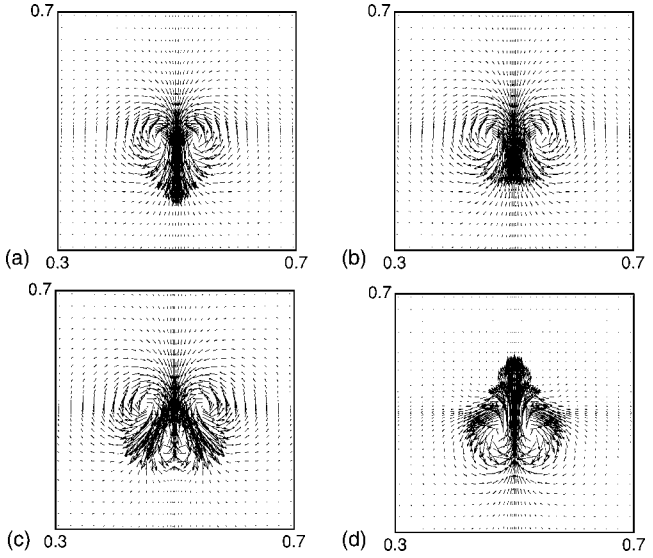

FIG. 3. Velocity fields around the heat source $\{(x,y)\in[0.3;0.7]^2\}$ in the case of Fig. 1(b) (higher frequency regime) at times (a) $t=\Delta t_{vib}+0.5$, (b) $t=\Delta t_{vib}+0.7$, (c) $t=\Delta t_{vib}+0.8$, and (d) $t=\Delta t_{vib}+1$.

First, after several periods of vibration, measurements have reported that the density field is not perfectly symmetrical. In Ref. [18] as in Ref. [19], the plumes appear wavy along their tails and perturbed at their heads. Figure 5 reports the density and velocity fields after more than 30 oscillations. At this time, density inhomogeneities generated by heating have been widely transported toward the top and bottom walls of

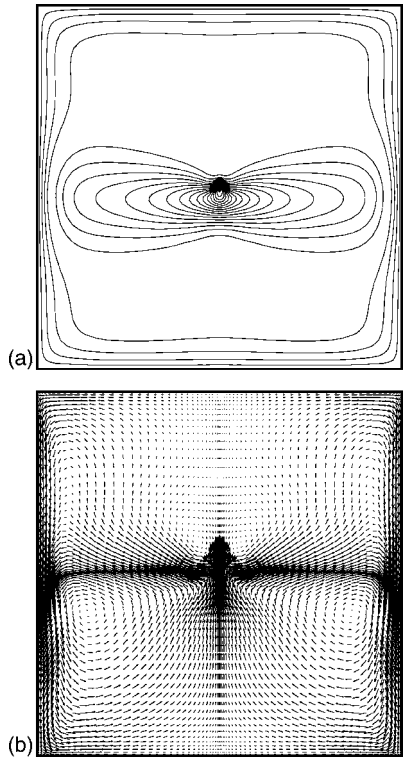

FIG. 4. Long-term behavior for the higher frequency regime. Density (a) and velocity (b) fields at $t'=\Delta t'_{vib}+40$ sec.

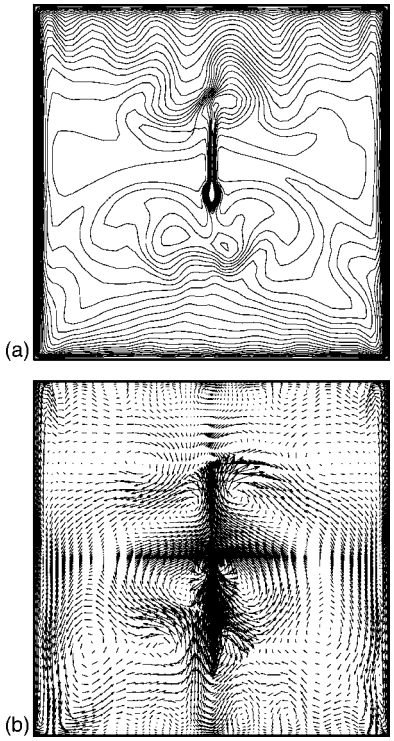

FIG. 5. Double-plume regime, long-term behavior. Density (a) and velocity (b) fields at $t' = \Delta t'_{vib} + 42.75$ sec.

the cavity, and fill almost all the domain (see the extension of isodensity lines from the horizontal boundaries). But the important feature at this point of our discussion is that the double plume has lost its symmetry in the vibration direction.

Two different mechanisms may explain such behavior. First, the velocity plot shows that many vortices are present in the flow. By itself, multiple vortex interplay can lead to flow destabilization and unpredictable dynamics [25]. The second set of noteworthy properties highlighted in Fig. 5 are related to the regular undulation of isodensity lines along the top wall. This pattern can be associated with a nascent Rayleigh-Bénard-like instability (with an oscillating gravity) developing from the top boundary layer, due to the presence of higher density fluid in this thermal boundary layer (every half period, this phenomenon is triggered in one horizontal boundary layer and then in the other) [20]. This then breaks the double-plume flow symmetry, as illustrated in Fig. 5. In Refs. [18,19], the flow symmetry breaking seems to appear sooner but, among the differences between the two situations, experiments were performed closer to the critical point, which favored the presence of steeper density gradients and thus could decrease the instability threshold. On the other hand, the interferometric image reported in Ref. [19] 120 sec after the beginning of the vibration also exhibits an undulation of the density field near the upper boundary, thus corroborating the development of a Rayleigh-Bénard-like instability along the wall's boundary layers.

The results presented in this paper give a short phenomenological explanation of some experimental observations performed a short time ago on near-critical fluid hydrodynamics in microgravity. They clearly exhibit the existence of two flow regimes depending on the frequency and amplitude of vibration. But heating intensity should obviously also be suspected of playing a role. Further developments in answering this question would be to determine the critical parameters ruling the emergence of one or the other of the two regimes.

[1] A. Onuki *et al.*, Phys. Rev. A **41**, 2256 (1990).
[2] H. Boukari *et al.*, Phys. Rev. A **41**, 2260 (1990).
[3] B. Zappoli *et al.*, Phys. Rev. A **41**, 2264 (1990).
[4] A. Onuki and R.A. Ferrell, Physica A **164**, 245 (1990).
[5] K. Nitsche and J. Straub, in ESA Report No. SP-256, 1987 (unpublished), p. 109.
[6] R.A. Ferrell and H. Hao, Physica A **197**, 23 (1993).
[7] B. Zappoli and P. Carlés, Eur. J. Mech. B/Fluids **14**, 41 (1995).
[8] A. Jounet *et al.*, Phys. Rev. Lett. **84**, 15 (2000).
[9] R.P. Behringer *et al.*, J. Low Temp. Phys. **81**, 71 (1990).
[10] P. Guenoun *et al.*, Phys. Rev. E **47**, 1531 (1993).
[11] J. Straub *et al.*, Phys. Rev. E **51**, 5556 (1995).
[12] F. Zhong and H. Meyer, Phys. Rev. E **51**, 3223 (1995).
[13] Y. Garrabos *et al.*, Phys. Rev. E **57**, 1 (1998).
[14] R.A. Wilkinson *et al.*, Phys. Rev. E **57**, 436 (1998).
[15] B. Zappoli *et al.*, J. Fluid Mech. **316**, 53 (1996).
[16] B. Zappoli *et al.*, J. Fluid Mech. **388**, 389 (1999).
[17] D. Bailly and B. Zappoli, Phys. Rev. E **62**, 2353 (2000).
[18] D. Beysens (unpublished).
[19] B. Zappoli *et al.*, Report No. IAF-00-T.6.10 (unpublished).
[20] S. Amiroudine *et al.*, J. Fluid Mech. (to be published).
[21] A. Jounet *et al.*, Phys. Fluids **12**, 197 (2000).
[22] S. Paolucci, Report No. SAND 82-8257, 1982 (unpublished).
[23] S. V. Patankar (unpublished).
[24] B. Zappoli (private communication).
[25] H. Aref, Annu. Rev. Fluid Mech. **15**, 345 (1983).